LAWRENCE
LIVERMORE
NATIONAL
LABORATORY

LLNL-TR-678550

# Simulation of Powder Layer Deposition in Additive Manufacturing Processes Using the Discrete Element Method

E. B. Herbold, O. Walton, M. A. Homel

October 26, 2015

This work performed under the auspices of the U.S. Department of Energy by Lawrence Livermore National Laboratory under Contract DE-AC52-07NA27344.

# Table of Contents

# Table of Figures

# 1 Introduction

## 1.1 Abstract

*This document serves as a final report to a small effort where several improvements were added to a LLNL code GEODYN-L to develop Discrete Element Method (DEM) algorithms coupled to Lagrangian Finite Element (FE) solvers to investigate powder-bed formation problems for additive manufacturing. The results from these simulations will be assessed for inclusion as the initial conditions for Direct Metal Laser Sintering (DMLS) simulations performed with ALE3D. The algorithms were written and performed on parallel computing platforms at LLNL. The total funding level was 3-4 weeks of an FTE split amongst two staff scientists and one post-doc. The DEM simulations emulated, as much as was feasible, the physical process of depositing a new layer of powder over a bed of existing powder.*

*The DEM simulations utilized truncated size distributions spanning realistic size ranges with a size distribution profile consistent with realistic sample set. A minimum simulation sample size on the order of 40-particles square by 10-particles deep was utilized in these scoping studies in order to evaluate the potential effects of size segregation variation with distance displaced in front of a screed blade. A reasonable method for evaluating the problem was developed and validated. Several simulations were performed to show the viability of the approach. Future investigations will focus on running various simulations investigating powder particle sizing and screen geometries.*

## 1.2 Experimental Background

Here we describe a discrete element method (DEM) simulation to evaluate the feasibility and utility of generating realistic particle-scale powder-bed configurations to investigate the additive manufacturing (AM) process. Of particular interest here is the laser cusing process, by which micron sized metallic particles are heated to above the melting point and welded by a precisely directed, narrow laser beam. The laser cusing process produces a thin layer of solidified material, which is then covered by more powdered metal particles pushed in front of a moving screed blade or roller. Figure 1 shows the Additive Manufacturing (AM) laser cusing process as depicted in [1]. The laser cusing AM process is also referred to as Direct Metal Laser Sintering (DMLS) or Selective Laser Melting (SLM) in the literature. The complete process is shown on the left side of Figure 1 including the powder reservoir on the left, which is emptied by a roller moving from left to right. The powder bed is lowered slightly to accommodate the new layer, which is typically a few particles thick. A blade perpendicular to the powder bed (shown on the right side of Figure 1) may also be used to screed powder particles across the fabrication bed.

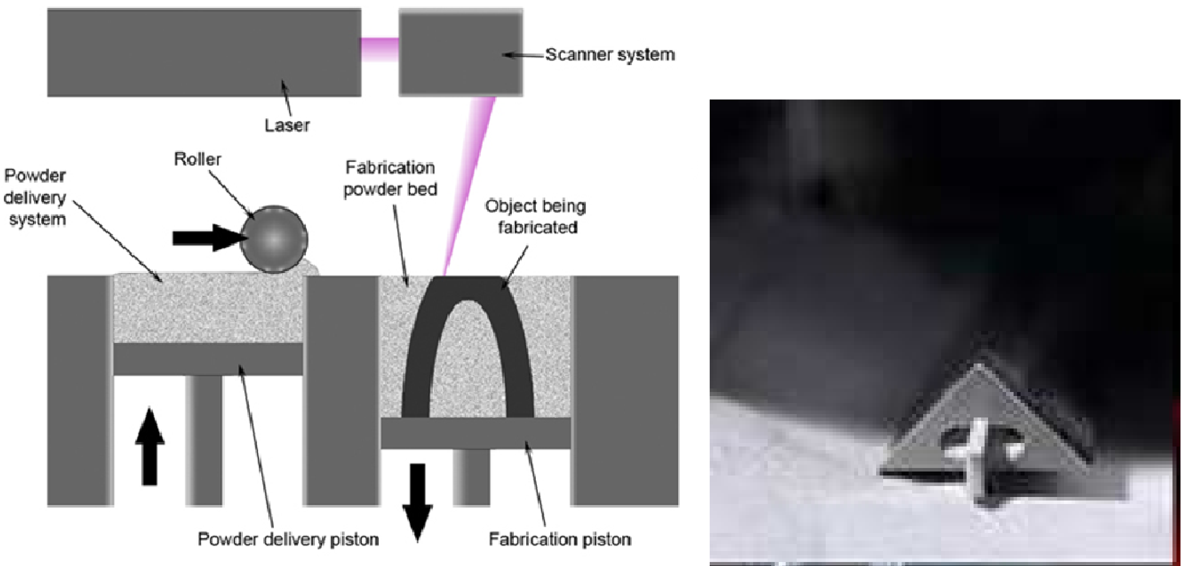


**Figure 1: The Additive Manufacturing (AM) laser cusing process as depicted in** [1]. **(left) The complete process is shown including the powder reservoir on the left, which is emptied by a roller moving from left to right. The powder bed is lowered slightly to accommodate the new layer, which is several particles thick. (right) A vertical blade may also be used to screed powder across the fabrication bed.**

The metallic powder particles used in laser cusing AM are typically less than 100 um and can nominally be composed of any metallic element or alloy amenable to melting within the laser power of the AM device. However, the quality of the final product depends highly on both the process control parameters related to the machine (e.g. screed speed, laser cusing speed, powder size, etc) as well as the powder material. For example, the laser cusing speed and direction has been investigated in [2] (see Figure 2) where Ti-6Al-4V powder particles (<100 um) are left intact as the scan rate approaches 1 m/s as shown in Figure 2 (c) and (d).

One of the attractive features of laser cusing AM techniques is that very little material is discarded (estimated at ~2% in [1]) in contrast to conventional machining where material is cut from a billet. This is true in theory, but it has been noted in [3] that the oxygen content may increase in recycled powder particles, the particle size distribution my increase [3,4] due to "satellite" particles (also known as slag in welding applications) as shown in Figure 3. It should be noted that the results of the investigation in [3] show that recycling Ti-6Al-4V powder particles up to 16x did not negatively affect the tensile strength of AM tensile specimens. It is important to investigate the effects of particle recycling, however, as tensile strength is not the only metric for part quality.

## 1.3 Numerical Modeling Background

A set of powder-bed formation DEM simulations were proposed to provide datasets allowing an evaluation of the magnitude and significance of differences among various beds of dry granular solids formed via simulated horizontal blades performing a screed-like spreading of layers of particles in a gravity field. The simulated particle bed configurations could also be compared to alternative particle-beds formed via a raining algorithm (which includes contact and algorithmically-prescribed subsequent rolling displacements to stable positions) or other methods where particles positions are optimized to find the densest packing within a prescribed domain. The DEM simulations were planned to emulate as much as is feasible the

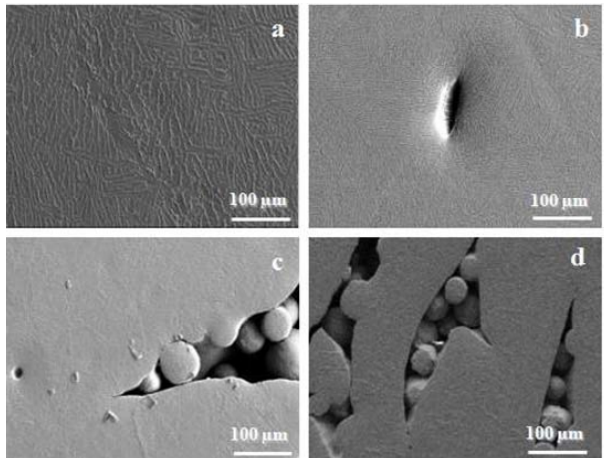


**Figure 2: Investigation of laser melt scans in Ti-6Al-4V powder from** [2]**. (a) and (c) show vertical scans, and (b) and (d) show horizontal scans. (a) and (b) are at a scan rate of 100 mm/s while (c) and (d) are at 1000 mm/s.**

physical process of depositing a new layer of powder over a bed of existing powder (including some slightly lower-elevation solid regions where the new solid body is being formed).

The DEM simulations described here utilize truncated size distributions (spanning realistic size ranges with a size distribution profile consistent with realistic sample sets). A minimum simulation sample size on the order of 40-particles square by 10-particles deep has been utilized in the scoping studies. In order to limit the scope of the simulations, the maximum simulated particle-bed dimension in the direction perpendicular to the screed travel direction was limited in the planned study to a value on the order of 100 particle diameters (or smaller).

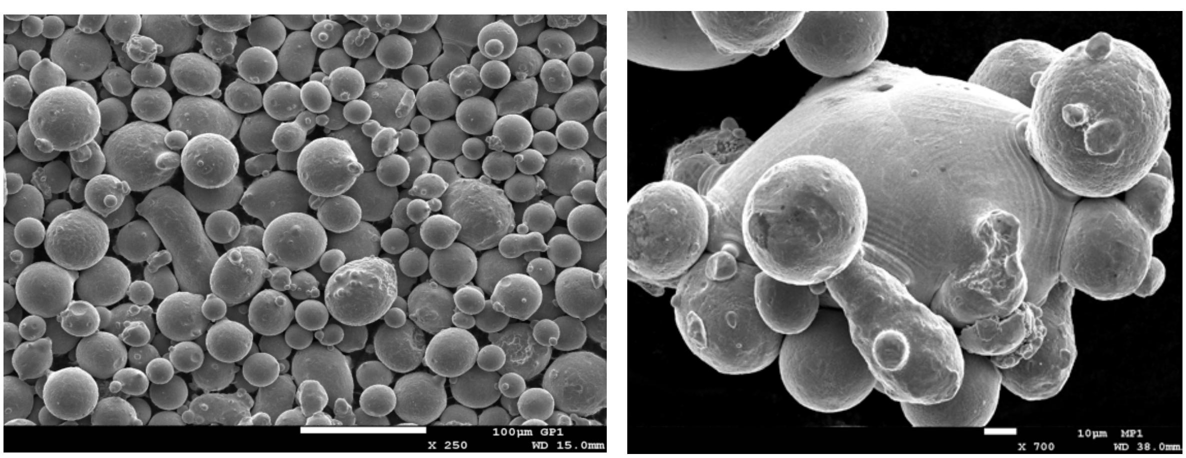


**Figure 3: SEM micrographs of recycled stainless steel particles. (left) particles are nominally spherical and some small particles are visibly welded to the surfaces of larger particles. (right) Large agglomerated particles may also be present in recycled powder.**

In addition to particle size distribution variables, the simulations are capable of varying the geometry of the simulated screed blade, and thus, could be utilized to examine a limited set of shapes, angles, and surface-stiffness and friction values, to determine sensitivity of the powder-bed response to screed-blade geometry and properties.

The goals of this demonstration simulation study were to:

- Demonstrate that DEM simulations can successfully be utilized to produce realistic powder beds with realistic size-segregation and packing distributions
- Produce representative powder bed configurations with different characteristics so that they can be evaluated in laser heating simulation studies (to test sensitivity of subsequent process steps to realistic variations in the particle-scale fabric of the initial powder bed)

### 1.3.1 Particle Shape

The Geodyn-L solver developed in in this investigation can handle ellipsoidal particles now (and other shapes can be added, if desired). A variety of non-spherical models exist in the various DEM codes used around the world. Among the non-spherical DEM codes often seen in the literature is the open-source LIGGGHTS DEM model, which is a derivative of the Sandia code, LAMMPS (with enhancements designed for granular materials). The non-spherical particle part of that 'enhancement' (i.e., rigid sphere-clusters) is not generally available as an 'open-source' code. Several other groups around the world have overlapping-sphere, or rigid-sphere-cluster DEM codes as well: e.g., Rudranarayan Mukherjee at JPL has been developing his own version of LAMMPS with non-spherical particles; Takashi Matsushima (U. Tsukuba, Japan) has had a sphere-cluster code for several years; Jerry Johnson & Anton Kulchitsky at the University of Alaska have parallelized Mark Hopkins' (CRREL) non-spherical particle DEM code; John Williams at MIT & Paul Cleary at CSIRO, Australia, both have DEM coses that use super-quartic shaped particles – the CSIRO group includes a gas-solid coupling mode. Commercial DEM codes with overlapping sphere-cluster particles include EDEM (DEM-Solutions) and Star-CCM+ (CD-Adapco).

### 1.3.2 Cohesion

Various models for cohesion exist in different DEM codes. For small, dry particles, the JKR representation of van der Waals force acting on elastically deformable spheres is probably the most widely accepted form that is also in a straightforward force-displacement representation, appropriate for DEM contact models; but various simplifications of that model are commonly used (since the original form of the JKR model is in a parametric form that usually requires interpolation in a table to evaluate). The cohesion model planned for this study is not an exact copy of the JKR force-displacement model, but the most important parameter, the pull-off force acting as two particle separate, can be set in the Geodyn-L cohesion model to a value corresponding to observed cohesive forces acting between ~20-micron scale spherical particles.

Theoretical estimates for the surface energy of stainless steel are typically in the range of 700 – 1100 $mJ/m^2$ [5]; however measured values of surface energy for rough, contaminated (i.e., air-exposed) stainless steel surfaces are more often in the range or 40-50 $mJ/m^2$ [6, 7]. The pull-off force based on the JKR [8] or DMT [9] interpretation of van der Waal interaction for contacting spherical particles (including elastic deformation) is given by

$$F_{p0}^{JKR} = \frac{3}{2}\pi\gamma R \qquad [\,1\,]$$

or

$$F_{p0}^{DMT} = 2\pi\gamma R. \qquad [\,2\,]$$

where $\gamma$ is the surface energy, and $R$ is the radius of curvature of the particles at their contact point (note that these two interpretations only differ by 33%, but the surface energy change from 'clean' to 'normal contamination' is factor of 20). One additional factor contributing to uncertainty in pull-off force is the surface morphology. The effective range of the van der Waals force is extremely small (decreasing by 2-orders of magnitude from its value when two smooth spheres are just touching to the value when they are only 20 – 40 *nm* apart. This means that 10 *nm* scale surface roughness can reduce the effective cohesion between particles, by keeping portions of the surface that would be in contact, separated by a small amount [10]. Based on the measured surface energy values (i.e., air-exposed) cited above and the JKR pull off force model, we can estimate the pull-off force for 25 *μm* stainless-steel spheres to be around 0.1*D* (*Newtons*) where *D* is the particle diameter in *meters* (e.g. 25 *μm* diameter particles would have a pull off force of around 2.5 *μN*, which is of the same order of magnitude, but slightly less than a single particle's weight, $W_p$~5*μN*).

The fact that interparticle pull-off forces are the same order of magnitude as an individual particle's weight is a warning flag that if particle size decreases by a factor of 2 or more, or the surface energy is larger than estimated, by a factor or 4 or more, then interparticle cohesion might begin to affect the bulk behavior of the powder (e.g. see [11]).

### 1.3.3 Stiffness

DEM simulations often use an effective modulus, which is up to 2 orders of magnitude lower than the elastic constants for the real material in the DEM force-displacement relation. This appears to be a large approximation, but it is standard practice for DEM simulations where the kinematics of the particle flow is the primary interest. This would not be correct if the actual forces on particles were the primary interest (e.g. if the interest was in knowing whether the particle-surfaces were receiving impact loads that would cause plastic deformation when they are flowing, etc.). In performing the simulations for this study it was found that the general character of the particle bed formation was not very sensitive to the modulus used. As a result, for the demonstration simulations, the modulus of the particles was reduced by around two orders of magnitude from that of smooth steel spheres. It is perhaps worth noting that for very low contact loads the surface morphology of asperities on the real physical spheres would also reduce the effective modulus of interaction, perhaps by a significant amount). Nonetheless, it would be appropriate to conduct a sensitivity study to confirm that the particle-bed configuration results are indeed nearly independent of the effective interparticle stiffness used in these simulations (i.e., over the stiffness range selected).

# 2 Powder Packing

A Monte-Carlo algorithm similar to [12] was implemented in GEODYN-L to pack the powders into the reservoir and working areas. This algorithm does not dynamically settle the particles, but creates an overly dense packing structure that is iteratively relaxed while extending one direction. This preferentially packs the particles similar to gravitational settling. The 'nominal' simulation 'sample' was constructed from a size distribution of spheres that is approximately a Gaussian distribution with a mean size of 27 *μm*, a full width at half maximum of 2.3 *μm*, and minimum and maximum cutoff diameters of 17 *μm* and 43 *μm*, respectively.

The minimum width of the simulation sample will be ~40 particle-diameters (i.e. around 1 *mm*) and the depth of the bed after spreading is anticipated to be ~3 particle diameters (i.e. 50

$\mu m$ - 70 $\mu m$), and the length of the 'travel' for creating the bed and/or spreading the bed was set as large as was practicable (based on patience and computer time).

The simulations in this initial study were intended to demonstrate a potential capability (but not to test the limits of what sample-size can be simulated). One of the goals of this simulation study was to include a large enough sample size to be able to determine whether the simulations can indicate the magnitude of size segregation or stratification that may be occurring in the direction of travel of the spreader blade.

The boundary conditions in Geodyn-L were modified so that a two-powder-bin system with a moving horizontal cylinder could scrape particle off of one bed and distribute them over the other (see Figure 8).

# 3 Implementation/Validation of Parallel DEM/FEM Solver in GEODYN-L

The Discrete Element Method (DEM) module of the LLNL code Geodyn-L was adapted for simulation of additive manufacturing powder spreading. Geodyn-L is an explicit Lagrangian FE code, which has previously been used for simulations of a wide variety of geotechnical problems, including simulations of the deflection of asteroids via hypervelocity impacts or interactions with nearby nuclear explosions. The cohesion and friction models in the code were originally developed to represent the behavior of initially cemented joints in rocks. Modifications have been made to those contact models so that they can realistically represent the behavior of small metal spherical particles interacting with each other and with other surfaces. DEM simulations of oblique impacts of ~20-micron steel spheres, using the modified inelastic, frictional contact representations, have been compared to previously run simulations of oblique impacts of elastic and elastic-perfectly-plastic spheres run using Dyna3D (i.e., a full FE representation of the colliding particles).

## 3.1 DEM Time Integration Scheme

The positions of each particle are computed by simple velocity Verlet time integration, which computes the velocities at the half time-step:

$$\dot{x}_{n+1/2} = \dot{x}_n + \ddot{x}_n \Delta t/2, \qquad [\,3\,]$$

to update the displacements at the end of the step assuming a constant velocity throughout the entire step:

$$x_{n+1} = x_n + \dot{x}_{n+\frac{1}{2}} \Delta t\ . \qquad [\,4\,]$$

The acceleration is computed from the contact forces, which depend on the updated positions

$$\ddot{x}_{n+1} = f(x_{n+1})/m, \qquad [\,5\,]$$

where

$$f(x_{n+1}) = f^{norm}(x_{n+1}) + f^{shear}(\dot{x}_{n+1/2}). \qquad [\,6\,]$$

The normal and shear components of the force are computed separately with,

$$f^{norm}(x_{n+1}) = k a_{n+1} \delta_{n+1}, \qquad [\,7\,]$$

and

$$f^{shear}\left(\dot{x}_{n+\frac{1}{2}}\right) = f^{shear}(\dot{x}_n) \cdot \left(\boldsymbol{I} - n_{cp}\right) + k_s a_{n+1} v_s \Delta t. \qquad [\,8\,]$$

The use of mixed time notations in Eq. [6] and [8] is allowed since the velocity is assumed constant over the step. The calculation of the relative slip of the particle surfaces is,

$$v_s = \dot{x}^+_{n+1/2} - \dot{x}^-_{n+1/2} + \omega^+_{n+1/2} \times \ell^+_{n+1/2} - \omega^-_{n+1/2} \times \ell^-_{n+1/2}. \qquad [\,9\,]$$

The relative slip velocity between the two surfaces accounts for the angular velocity ($\omega$) and the distance from the particle center to the contact point ($\ell$). The contact area ($a$) and displacement overlap ($\delta$) are computed from the position and radii (or local radii as it were),

$$a_{n+1} = \pi\sqrt{R_{eff}\delta_{n+1}/2}\,, \qquad [\ 10\ ]$$

$$R_{eff} = \left(\frac{1}{R^+} + \frac{1}{R^-}\right)^{-1}, \qquad [\ 11\ ]$$

$$\delta_{n+1} = \left\|x^+_{n+1/2} - x^-_{n+1/2}\right\| - (R^+ + R^-)\,. \qquad [\ 12\ ]$$

The angular positions and velocities of the particles are integrated according to the quaternion update described in [6]. The shear force in Eq. [8] is used to compute the torque at the half time-step,

$$\tau_{n+1/2} = \ell_{n+1/2} \times f^{shear}\left(\dot{x}_{n+\frac{1}{2}}\right).$$

The angular accelerations are found using the torques and angular velocity estimates at the half time-step, though the details for computing $\omega_{n+1/2}$ are omitted for brevity since it is detailed in [13],

$$\dot{\omega}_{n+1/2} = I^{-1}(\tau_{n+1/2} - \omega_{n+1/2} \times I\omega_{n+1/2}), \qquad [\ 13\ ]$$

where *I* is the particle moment of inertia. The angular velocity is then updated assuming a constant angular acceleration over the step (in a frame of reference rotated to the principal body axes). The unit quaternion is updated to the end of the step through

$$q_{n+1} = \left[\cos\frac{\|\omega_{n+1/2}\|\Delta t}{2}, \sin\frac{\|\omega_{n+1/2}\|\Delta t}{2}\frac{\omega_{n+1/2}}{\|\omega_{n+1/2}\|}\right] q_n. \qquad [\ 14\ ]$$

Finally, the velocity at the end of the step is computed to complete the time-step,

$$\dot{\boldsymbol{x}}_{\boldsymbol{n+1}} = \dot{\boldsymbol{x}}_{\boldsymbol{n+1/2}} + \ddot{\boldsymbol{x}}_{\boldsymbol{n+1}}\boldsymbol{\Delta t/2}. \qquad [\ 15\ ]$$

The critical time-step is computed from the stiffness at the contact and effective mass of the contacting particles with,

$$\Delta t = 2\pi c_1\sqrt{\frac{m^+m^-}{k(m^+ + m^-)}}.\,. \qquad [\ 16\ ]$$

Where c1 is a constant provided as a parameter.

## 3.2 Contact/Friction/Cohesion Model

Appropriate viscous damping coefficient values for the modified DEM force-displacement model were able to produce coefficient-of-restitution values that are similar to the elastic-perfectly-plastic Dyna3D simulations, and the frictional coupling model produced changes in rotational and translational motion of the colliding particles consistent with those produced by Dyna3D (i.e., including a sticking, or rolling, condition for near-normal impacts, a sliding condition for highly oblique impacts, and a gradual transition from sliding to rolling behavior that is nearly identical whether the collision is simulated via the simple DEM contact force-displacement model in Geodyn-L, or using the fine-grid FEM representation in the Dyna3D simulation, which included thousands of grid cells in the contact region).

The viscous damping term in the Geodyn-L contact model approximates the kinetic energy loss to plastic deformation in normal-direction impacts – it is not an exact representation of the process, but provides appropriate dissipation of kinetic energy for collisions. Figure 4 shows the variation of the coefficient of restitution for normal-direction impacts between two equal size spheres as a function of incident velocity as calculated by the DEM module in Geodyn-L, using a viscosity coefficient of 40. The Dyna-3D simulations of collisions between 20µm elastic-

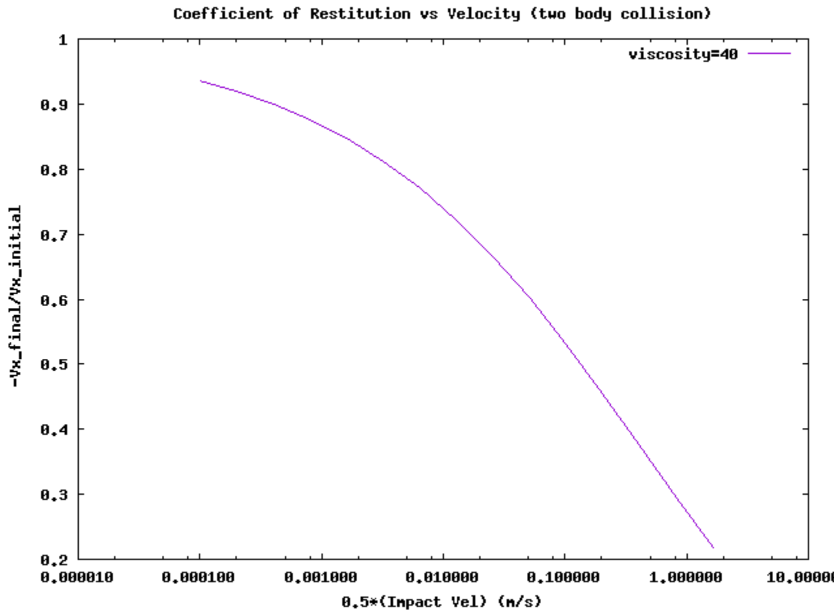


**Figure 4: Normal-direction coefficient of restitution vs impact velocity for collisions between 25µm steel spheres modeled in Geodyn-L with a viscosity parameter value of 40. For impact velocities in the range of 2 to 5 mm/s these restitution values are close to those obtained in Dyna3D FEM simulations of 20 µm elastic-plastic spheres colliding [14].**

plastic steel spheres resulted in a normal direction coefficient of restitution of around 0.9 for an impact velocity of 2mm/s, and 0.8 for an impact speed of 5mm/s. These values are the same order of magnitude as those shown in Figure 4 using the Goedyn-L DEM module with viscosity coefficient of 40. Since the primary aim of the larger-scale simulation study (shown later) was to demonstrate general capability of this type of simulation, higher values of velocity for screed blades were used in the simulations (in order to reduce total computational time) than are likely used in real powder distribution scenarios. Consequently, a higher viscosity coefficient was used in the simulations to more-rapidly dissipate kinetic energy as the particles interacted with the stationary bed layer.

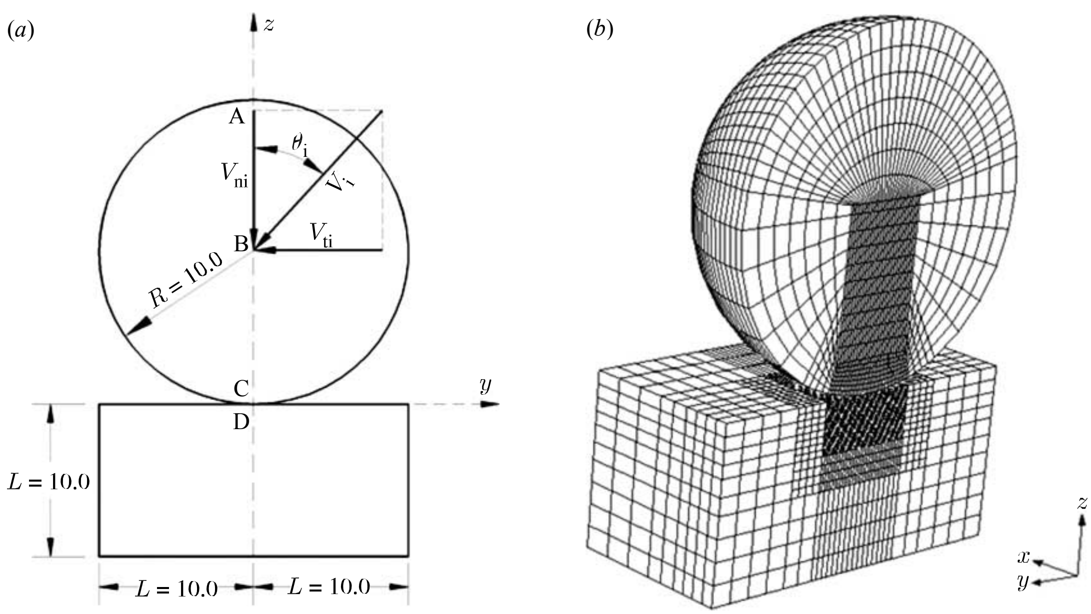


**Figure 5: Dyna3D FE model for the oblique impact of a sphere with a half-space (units in [mm]): (a) the model and (b) the finite-element meshes [14].**

**Table 1: Material properties in oblique impact [14].**

| material property | *E* (GPa) | n | *Y* (GPa) | ρ (g/cm$^3$) |
|---|---|---|---|---|
| elastic | 208.0 | 0.3 | — | 7.85 |
| elastic, perfectly plastic | 208.0 | 0.3 | 1.85 | 7.85 |

The contact friction models in Geodyn-L were tested for oblique collisions of pairs of 20 to 30 micron steel spheres and compared the resulting changes in translation and rotation with published Dyna3D simulations [14] of oblique impacts between the same-scale steel spheres, and obtained reasonable agreement as shown in Figure 6, confirming that the friction model adapted from the geologic contact model already in the code is producing the kind of results we want for small metal spheres.

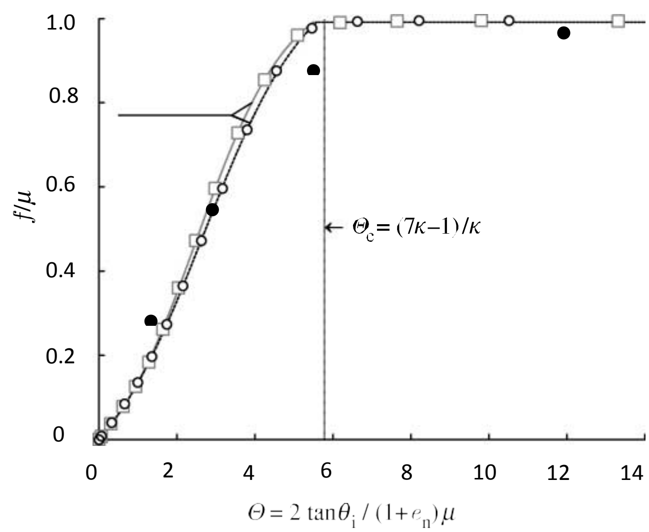


**Figure 6: The variation of $f/\mu$ with the dimensionless impact angle for PE impact with various initial impact velocities. This ratio is that of tangential to normal impulse divided by the coefficient of friction. Squares, $v_{ni}$=2.0 mm/s, circles, $v_{ni}$=5.0mm/s [14], filled circles Geodyn-L DEM module two-particle collision simulations.**

### 3.2.1 Other simulation considerations

The DEM model in Geodyn-L does not currently include 'rolling resistance' at the contacts (most DEM models do not include that effect). If cohesion becomes large, or the particles get much smaller than 20-microns, then that mode of motion may become important (and rolling-resistance might need to be added). There were no plans to add that capability in this initial feasibility demo study. Only if the model is not able to match powder flow or spreading behavior, would we plan to add rolling resistance, in the future (it is not difficult to add this feature, but would probably take more than a week of effort to put in, debug and verify). Similarly, non-spherical particles could also be included if the shape effects appear important – but that was not part of the plan for this study.

### 3.2.2 Stiffness

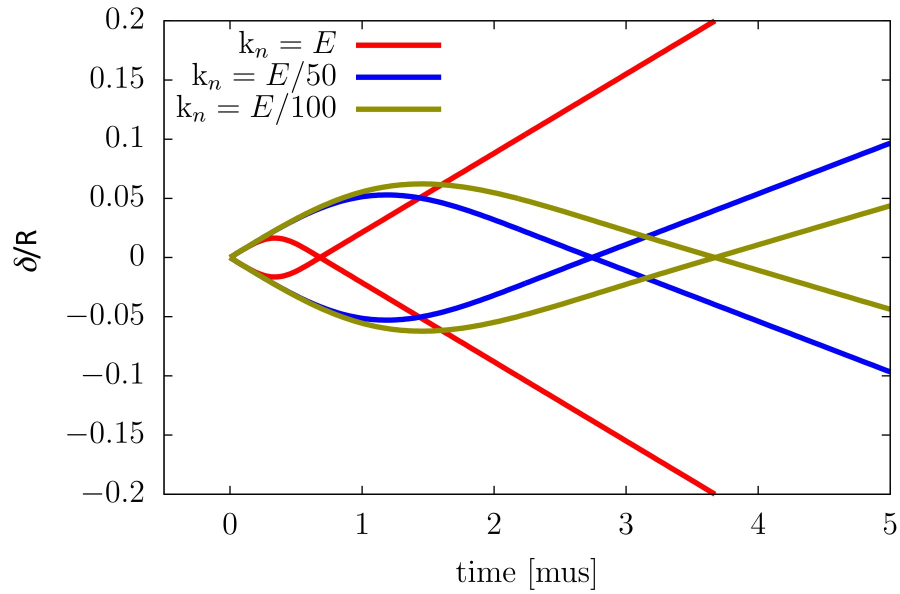


**Figure 7: Impact simulation of two particles at 1m/s for three different stiffness values. The fraction of displacement with respect to the particle radius (R=15um) is shown as a function of time. The elastic modulus of stainless steel E=200 GPa is used as the nominal stiffness value between powder particles. Two different values of E/50 and E/100 are also used in an attempt to increase the time-step without adversely affecting the results of the simulation. Since the simulation runs for tens of millions of timesteps due to the slow process of screed deposition, it is important to evaluate the effects of adjusting material parameters on the stability of the simulations.**

As discussed above, the full spreading simulations in this study utilized particles that had their stiffness reduced by a factor of approximately 100 from the modulus of stainless steel. In order to determine what whether or not such a stiffness reduction (done to allow larger time steps in the numerical integration equations) would have a significant effect on the kinematics of the particle bed formation we examined the overlap that would occur at relatively high impact velocities (a general rule of thumb for DEM simulations is to keep the computational-particle stiffness a range where the particle overlaps are less than 1% of particle diameters, in order to avoid kinematic behavior that is unrepresentative of the 'real' particles being simulated). Figure 7 shows the displacement time history of colliding spheres using various stiffness reduction values for a collision incident velocity of ~1 m/s. This velocity is higher than any expected velocity in the spreading simulation, and this 2-particle collision simulation indicates that if velocities approach 1 *m/s*, the simulations will likely include some minor deviation from realistic behavior because overlaps in the simulations will be as high as 5% of the particle diameters. For velocities on the order of 1 cm/s we would expect that the 100X reduction in particle stiffness will have only a very minor effect on bulk flow kinematics; however, prudent simulation practice would suggest that a sensitivity study confirm that the stiffness reduction does not produce a significant change in the resulting powder bed configurations. It might be noted that real particle contact stiffness is often softer than that of ideal smooth spheres initially, because asperity deformation dominates in low velocity impacts (at high velocities the contact area gets large compared to asperity size, so that argument is no longer valid).

# 4 Results

Appropriate moving boundary models were set up in the new DEM module to represent powder spreading for additive manufacturing applications. The results of the packing algorithm in parallel are shown in Figure 8 along with the finite element mesh for the bounding continuous solid bodies. In the top portion of Figure 8 half of the screed blade is visible as a light gray mesh. This mesh represents the right side of Figure 1 where the vertical blade projects down from a horizontal beam with a triangular cross-section. In the bottom part of Figure 8 a roller is shown. The roller is meshed with hexahedral finite elements. In both cases, the elements are rigidly translated across the reservoir and the particles are deposited into the target area. The colors of the particles in Figure 8 indicate the processor number. The simulations were tested on 8 and 16 processors. The use of a greater number of processors did not appreciably increase the speed of the simulation.

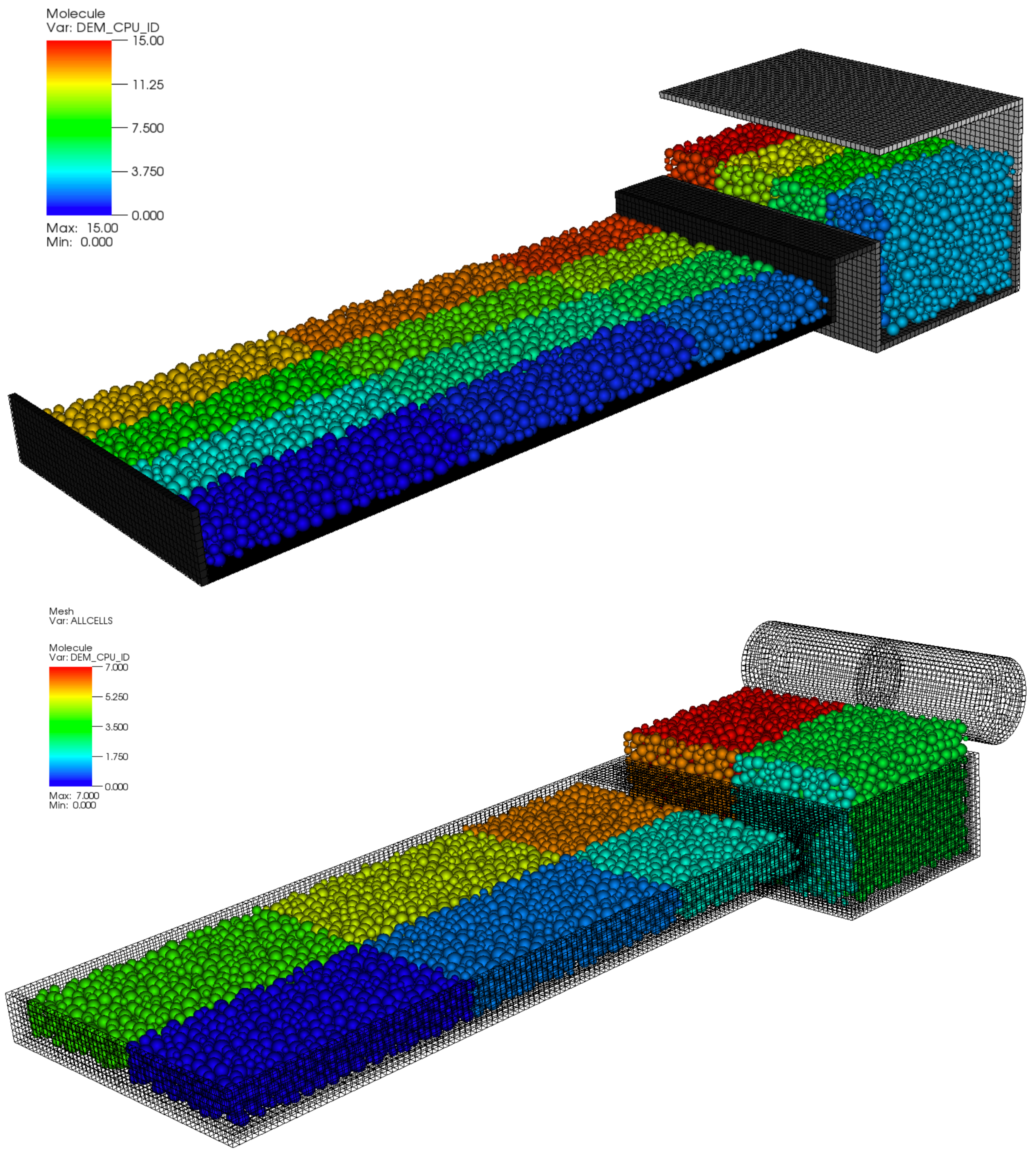


**Figure 8: Initial configuration of roller mesh and the powder reservoir and particle bed.**

Several snapshots of one of the simulations are shown in Figure 8. The powder particles piled up to the top part of the blade and then moved forward at 1 cm/s towards the target area. This process effectively mixed the particles since they collectively experienced a shear deformation as they turned the corner at the top of the blade. The particles eventually deposit on the target bed and the remaining pile is again sheared across the top of the deposited layer by the bottom of the screed blade.

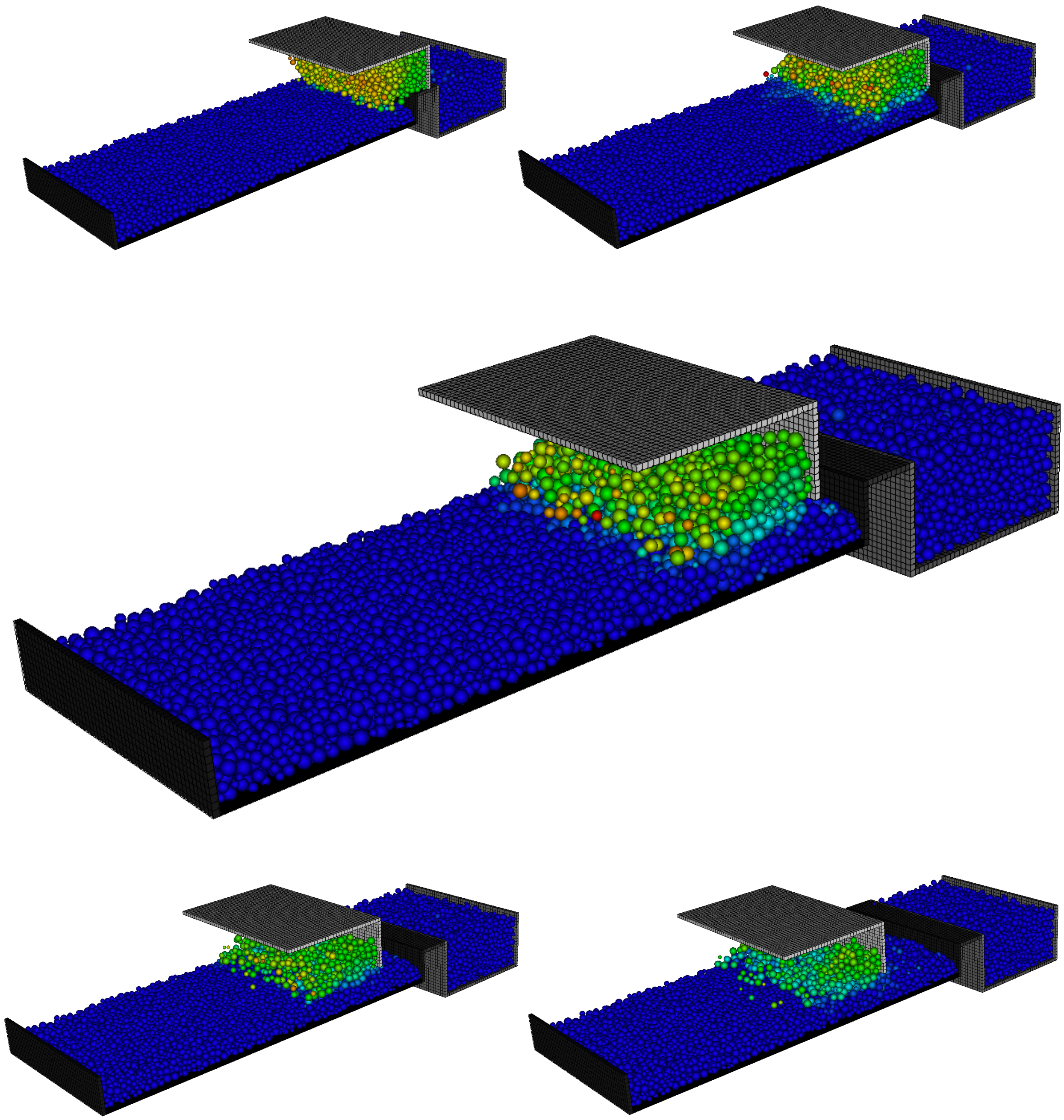

**Figure 9: Particle deposition GEODYN-L simulation with 14,105 DEM powder grains on 16 cpus. The time in the final frame is $t_f$ = 0.028 s. The color gradient shows the particle speed from 0-1 cm/s.**

The particles from the reservoir and target area were given different group identifications allowing one to distinguish the mixing between the particles from the different groups. Figure 10 shows that although the top of the deposited layer is relatively flat due to the passage of the screed blade, the interfacial layer between the two particle groups is undulated. This is, in part, due to the impact of the powder onto the target area after falling from the separating section. However, one can see that this also produces a piling of the particles from the target area and may entrain these particles within the deposition layer.

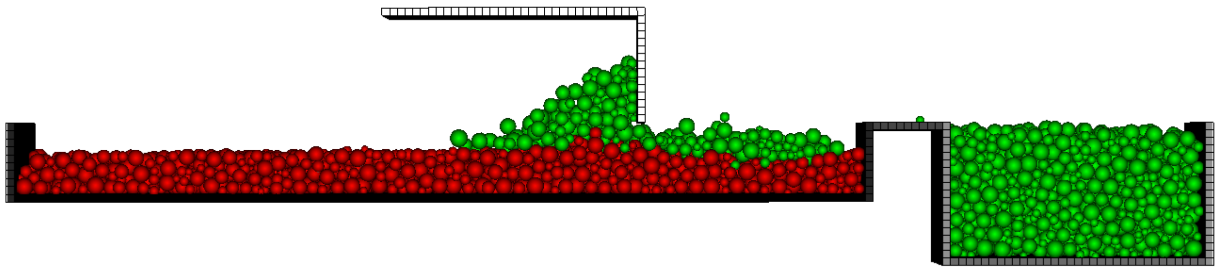

**Figure 10: Sideview of GEODYN-L simulation showing how the particles deposit from the reservoir to the fabrication area. The two color scheme shows that the line between the two layers of particles is not flat indicating that mixing may be important during deposition.**

For a better depiction of the undulating target layer, Figure 11 shows a heightmap of the target layer particles with the reservoir particles removed. It is clear that some of the particles from the target layer are beginning to mix in with the particles from the reservoir.

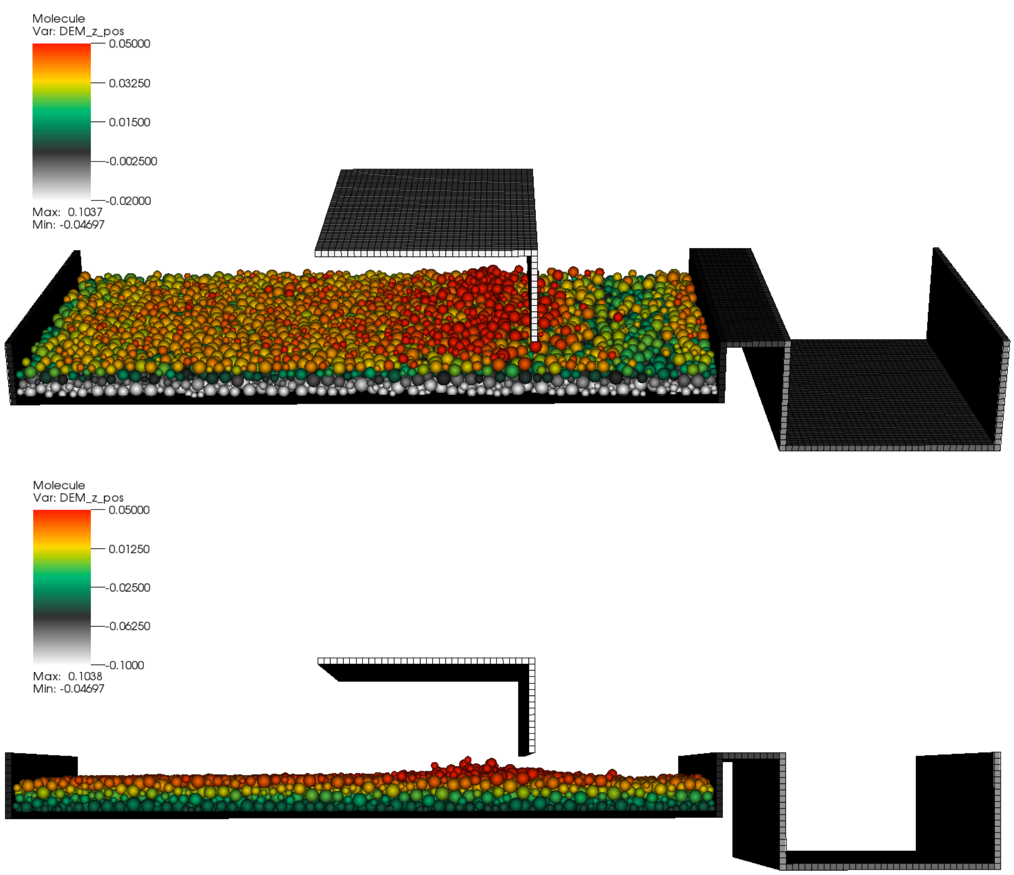


**Figure 11: Two different perspectives showing the side-view showing only particles within the initial target area. Some of these particles have been scraped up into the deposition mass and are dragged forward as the rest of the layer is deposited.**

Thus, we have identified two sources of mixing from the vertical screed deposition process:

1. mixing due to lifting/piling particles from the powder reservoir
2. mixing due to impact or particle scraping, which may produces an undulating interfacial layer.

These two mechanisms of mixing may be important control factors when assessing the repeatability and quality of AM laser cused parts.

# 5 Future Development

We implemented the DEM/FEM contact in parallel and tested GEODYN-L such that the particles were repartitioned across CPU's as they moved through space to reduce intercommunication times. The data structure was written generally to handle ellipsoidal particles or angular faceted shapes, but the contact algorithm for those shapes was not verified or validated here. Future developments could include the inclusion of verification/validation of the DEM/FEM coupling for differently shaped DEM particles. Secondly, cohesion must be treated differently than cohesive contacts typically used for finite element calculations between element surfaces. The cohesive model should be verified and validated further to enable an estimate of its effects on the mixing observed in these simulations (with or without frictional losses). Although the pull-off force expected to exist between the AM-sized particles was estimated from literature values of measured surface energies, the simulations performed did not include any interparticle cohesive forces.

# 6 Conclusions

The DEM simulations utilized truncated size distributions (spanning realistic size ranges with a size distribution profile consistent with realistic sample sets). A minimum simulation sample size on the order of 40-particles square by 10-particles deep was utilized in these scoping studies in order to evaluate the potential effects of size segregation variation with distance displaced in front of the screed blade. A reasonable method for evaluating the problem was developed and validated. Several simulations were performed to show the viability of the approach. Future investigations would focus on running various simulations investigating powder particle sizing and screen geometries.

This work was performed under the auspices of the U.S. Department of Energy by Lawrence Livermore National Laboratory under Contract DE-AC52-07NA27344. This work was funded by the Laboratory Directed Research and Development Program at LLNL under project tracking code 13-SI-002.

# 7 References

[1] KARMA. Detailed Report on Laser Cusing , SLA , SLS and Electron Beam Melting (including Technical, Economical and Safety Features). 2008.

[2] Puebla K, Murr LE, Gaytan SM, Martinez E, Medina F, Wicker RB. Mater Sci Appl 2012;03:259.

[3] Tang HP, Qian M, Liu N, Zhang XZ, Yang GY, Wang J. Jom 2015;67:555.

[4] Slotwinski J a, Garboczi EJ, Stutzman PE, Ferraris CF, Watson SS, Peltz M a. J Res Natl Inst Stand Technol 2014;119:460.

[5] www.markingsystems.com/pdf/3mfundamentals_of_adhesion.pdf

[6] Santos, O., T. Nylander, R. Rosmaninho, G. Rizzo, S. Yiantsios, N. Andritsos, A. Karabelas, H. Müller-Steinhagen, L. Melo, L.Boulangé-Petermann, C. Gabet, A. Braem, C. Trägårdh, M. Paulsson (2004) "Modified stainless steel surfaces targeted to reduce fouling – surface characterization," *J. of Food Engineering* **64** p63-79.

[7] Hedberg, Y., M-E. Karlsson, E. Blomberg, I. O. Wallinder, J. Hedberg (2014) "Correlation between surface physicochemical properties and the release of iron from stainless steel AISI 304 in biological media," *Colloids and Surfaces B: Biointerfaces,* **122** p216-222

[8] Johnson, K. L., K. Kendall and A. D. Roberts, *Proc. R. Soc. Lond.* A324, 301–313 (1971)

[9] Derjaguin, BV, VM Muller, and Y.P.Toporov (1975) "Effect of contact deformations on the adhesion of particles," *Journal of Colloid and Interface Science*, **53**(2), pp. 314-326.

[10] Walton, O.R. (2008) "Review of Adhesion Fundamentals for Micron-Scale Particles," *Kona* (**26**) pp129-141.

[11] Walton, O.R., C.P. De Moor, K.S. Gill (2007) "Effects of gravity on cohesive behavior of fine powders: implications for processing Lunar regolith," *Granular Matter* **9**:353-363.

[12] He D, Ekere NN, Cai L. Phys Rev E 1999;60:7098.

[13] Zhao F, van Wachem BGM. Acta Mech 2013;224:3091.

[14] Wu, C-Y, C. Thornton, and L-Y Li (2009) "A semi-analytical model for oblique impacts of elastoplastic spheres," *Proc. Roy. Soc. A* **465**, p937-960.